JACS
JOURNAL OF THE AMERICAN CHEMICAL SOCIETY
Article
pubs.acs.org/JACS

# UTSA-74: A MOF-74 Isomer with Two Accessible Binding Sites per Metal Center for Highly Selective Gas Separation

Feng Luo,[†] Changsheng Yan,[†] Lilong Dang,[†] Rajamani Krishna,[‡] Wei Zhou,[§] Hui Wu,[§] Xinglong Dong,[∥] Yu Han,[∥] Tong-Liang Hu,[⊥] Michael O'Keeffe,[#] Lingling Wang,[†] Mingbiao Luo,[†] Rui-Biao Lin,[▽] and Banglin Chen*[,▽]

[†]School of Biology, Chemistry and Material Science, East China University of Technology, Fuzhou, Jiangxi 344000, China
[‡]Van't Hoff Institute for Molecular Sciences, University of Amsterdam, Science Park 904, 1098 XH Amsterdam, The Netherlands
[§]Center for Neutron Research, National Institute of Standards and Technology, Gaithersburg, Maryland 20899-6102, United States
[∥]Advanced Membranes and Porous Materials Center, Physical Sciences and Engineering Division, King Abdullah University of Science and Technology, Thuwal 23955-6900, Saudi Arabia
[⊥]School of Materials Science and Engineering, National Institute for Advanced Materials, Collaborative Innovation Center of Chemical Science and Engineering (Tianjin), Nankai University, Tianjin 300071, China
[#]School of Molecular Sciences, Arizona State University, Tempe, Arizona 85287, United States
[▽]Department of Chemistry, University of Texas at San Antonio, One UTSA Circle, San Antonio, Texas 78249-0698, United States

Supporting Information

**ABSTRACT:** A new metal−organic framework $Zn_2(H_2O)$-(dobdc)·0.5($H_2O$) (**UTSA-74**, H4dobdc = 2,5-dioxido-1,4-benzenedicarboxylic acid), Zn-MOF-74/CPO-27-Zn isomer, has been synthesized and structurally characterized. It has a novel four coordinated **fgl** topology with one-dimensional channels of about 8.0 Å. Unlike metal sites in the well-established MOF-74 with a rod-packing structure in which each of them is in a five coordinate square pyramidal coordination geometry, there are two different $Zn^{2+}$ sites within the binuclear secondary building units in **UTSA-74** in which one of them (Zn1) is in a tetrahedral while another (Zn2) in an octahedral coordination geometry. After activation, the two axial water molecules on Zn2 sites can be removed, generating **UTSA-74a** with two accessible gas binding sites per Zn2 ion. Accordingly, **UTSA-74a** takes up a moderately high and comparable amount of acetylene (145 $cm^3/cm^3$) to Zn-MOF-74. Interestingly, the accessible $Zn^{2+}$ sites in **UTSA-74a** are bridged by carbon dioxide molecules instead of being terminally bound in Zn-MOF-74, so **UTSA-74a** adsorbs a much smaller amount of carbon dioxide (90 $cm^3/cm^3$) than Zn-MOF-74 (146 $cm^3/cm^3$) at room temperature and 1 bar, leading to a superior MOF material for highly selective $C_2H_2/CO_2$ separation. X-ray crystal structures, gas sorption isotherms, molecular modeling, and simulated and experimental breakthroughs comprehensively support this result.

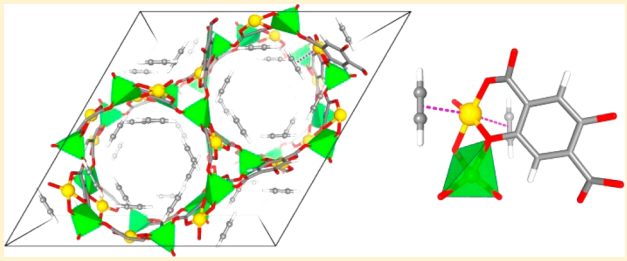

## INTRODUCTION

Porous metal−organic frameworks (MOFs) have a variety of different applications for gas storage, separation, sensing, heterogeneous catalysis, drug delivery, bioimaging, and photonics because of their unique pore structures and surfaces.[1−4] They can be easily self-assembled from simple metal salts and organic linkers. The richness of both inorganic and organic components for the construction of MOFs has provided us enormous opportunities to synthesize a large number of MOF materials whose pore sizes, pore surface functions, and pore volumes can be systematically tuned for the above-mentioned specific applications. Among the diverse MOFs examined, some prototypical MOFs, as exemplified by MOF-5 (IRMOF-1),[5] HKUST-1,[6] $Cu(4,4'\text{-bipy})_2(SiF_6)$,[7] MOF-74,[8] ZIF-8,[9] MIL-101,[10] and UiO-66,[11] have played very important roles in the development of MOF chemistry and materials because of their unique pore structures. MOF-74 series are characteristic of the highest density of open metal sites on the 1D channel pore surfaces of about 11 Å.[12] Furthermore, different metal sites such as $Mg^{2+}$, $Zn^{2+}$, $Ni^{2+}$, $Co^{2+}$, $Mn^{2+}$, $Fe^{2+}$, and $Cu^{2+}$ can be systematically immobilized into their pore surfaces of the corresponding isostructural MOFs for their different molecular recognition and/or chemical transformations.[13] Accordingly, they have the record performance for the postcombustion carbon dioxide capture,[14] acetylene[15] and methane storage,[16] and light hydrocarbon separations,[17] as well as some very specific gas separations such as $O_2/N_2$,[18] $CO/H_2$, and $CO/N_2$.[19] The open Fe(II) sites can be utilized as the cocatalytic sites for the oxidative

**Received:** February 23, 2016
**Published:** April 26, 2016





DOI: 10.1021/jacs.6b02030
J. Am. Chem. Soc. 2016, 138, 5678−5684

transformation of ethane to ethanol[20] and the release of nitric oxide.[21] The pores within MOF-74 are very robust, so they have been examined as the host materials to illustrate the gas sorption mechanisms through the adsorbate superlattice formation.[22] The open metal sites can be postfunctionalized to tune the pores and to introduce functional sites, particularly amine sites, for their postcombustion carbon dioxide capture and separations.[23] Its expanded organic linkers have also led to isoreticular MOFs whose pores are systematically enlarged up to about 100 Å for the encapsulation of enzyme molecules.[24] Because of the significance of this series of MOFs, the community has been considering the possibility to construct new functional isomeric MOFs from the same organic linker 2,5-dioxido-1,4-benzenedicarboxylic acid but without success.

Ideal porous materials for column breakthrough gas separations are those which can not only take up a large amount of the preferred gas molecule but also display significantly high gas separation selectivity.[25] Those exhibiting high sieving effects can meet the high gas selectivity; however, their small pores typically limit their gas uptakes.[26] On the other hand, those taking up large amount of gas molecules generally have comparatively low gas separation selectivity.[17] This is the so-called trade-off between physical adsorption capacity and selectivity of porous materials, a daunting challenge to developing porous materials for gas separations. During our exploration of new multifunctional MOF materials, we discovered a new isomeric Zn-MOF-74, $Zn_2(H_2O)(dobdc)\cdot 0.5(H_2O)$ ($H_4$dobdc = 2,5-dioxido-1,4-benzenedicarboxylic acid); we term **UTSA-74**), which motivated us to examine its potential for gas storage and separations. Unlike Zn-MOF-74 with the rod-packing structure, **UTSA-74** has a discrete binuclear Zn cluster as the secondary building unit and a novel four coordinated **fgl** topology with one-dimensional pore channels of about 8.0 Å, smaller than 11 Å in Zn-MOF-74. There exist two different $Zn^{2+}$ atoms in **UTSA-74**: (a) tetrahedral and saturated Zn1, and (b) octahedral Zn2 with two accessible sites per metal center. Accordingly, the structure of **UTSA-74** is significantly different from the well-known Zn-MOF-74. Gas sorption studies indicate that **UTSA-74** takes up a large amount of acetylene of 152 $cm^3/cm^3$ under ambient conditions, which is comparable to that of Zn-MOF-74; however, to our great surprise, **UTSA-74** adsorbs a much smaller amount of carbon dioxide (90 $cm^3/cm^3$) than Zn-MOF-74 (146 $cm^3/cm^3$). As a result, **UTSA-74** can have both high gas adsorption capacity and gas separation selectivity for the separation of $C_2H_2/CO_2$, breaking the trade-off rule of porous materials for gas separation and demonstrating itself as a superior porous adsorbent for column breakthrough separation of $C_2H_2/CO_2$ under ambient conditions. Single crystal X-ray structures of the as-synthesized **UTSA-74**, activated **UTSA-74a**, and carbon dioxide included **UTSA-74⊃$CO_2$**; molecular modeling studies; and simulated and experimental breakthroughs have conclusively supported the claim.

## EXPERIMENTAL SECTION

**Materials and Physical Measurements.** The commercial chemicals are used as purchased from Alfa. Thermogravimetric analysis (TG) was performed by a TGA Q500 thermal analysis system. All TGA experiments were performed under a $N_2$ atmosphere from 40 to 800 °C at a rate of 5 °C/min. Data were analyzed using the TA Universal Analysis software package. X-ray powder diffraction were collected by a Bruker AXSD8 Discover powder diffractometer at 40 kV, 40 mA for Cu K$\alpha$ ($\lambda$ = 1.5406 Å).

The gas sorption isotherms were collected on a Belsorp-max. Ultrahigh-purity-grade (>99.999%) $N_2$, $CO_2$, and $C_2H_2$ gases were used in this adsorption measurement. To maintain the experimental temperatures, liquid nitrogen (77 K) and a temperature-programmed water bath (273 and 298 K) were used, respectively.

**Synthesis of UTSA-74.** A mixture of $H_4$dobdc (0.099 g, 0.50 mmol), $Zn(NO_3)_2\cdot 6H_2O$ (0.149 g, 0.50 mmol), *N*,*N*′-dimethylformamide (DMF, 6.0 mL), and $H_2O$ (0.20 mL) was placed in a Teflon-lined stainless steel vessel (12 mL) and heated at a rate of 1 °C $min^{-1}$ to 158 °C, and kept at that temperature for 72 h, and then it was cooled to room temperature at a rate of 0.1 °C $min^{-1}$. Subsequently, yellow rod-shaped crystals were obtained in an 89% yield based on $Zn(NO_3)_2\cdot 6H_2O$. Anal. Calcd for $Zn_2(H_2O)(dobdc)\cdot 0.5(H_2O)$-$(C_8H_5O_{7.5}Zn_2)$: C, 27.30; H, 1.43; N, 0.00. Found: C, 27.21; H, 1.47; N: 0.06.

**X-ray Crystallography.** X-ray diffraction data were collected on a Bruker-AXS SMART Breeze CCD diffractometer at 296 K for **UTSA-74** and **UTSA-74a** and at 120 K for **UTSA-74⊃$CO_2$** using graphite monochromated Mo K$\alpha$ radiation ($\lambda$ = 0.710 73 Å). Preparation of **UTSA-74⊃$CO_2$** crystals follows: The as-synthesized crystals of **UTSA-74** were placed into the sample holder and activated to remove solvent molecules in situ using the gas adsorption apparatus Belsorp-max at 200 °C under high vacuum for 2 h to generate the crystals of activated **UTSA-74a**. Gradual loading of $CO_2$ into the **UTSA-74a** sample up to 100 kPa at 298 K leads to the formation of crystals of **UTSA-74⊃$CO_2$**, which were transferred into glovebox, and sealed into the capillary tubes under $CO_2$ atmosphere. The data reduction included a correction for Lorentz and polarization effects, with an applied multiscan absorption correction (SADABS). The crystal structure was solved and refined using the SHELXTL program suite. Direct methods yielded all non-hydrogen atoms, which were refined with anisotropic thermal parameters. All hydrogen atom positions were calculated geometrically and were riding on their respective atoms. The SQUEEZE subroutine of the PLATON software[27] suite was used to remove the scattering from the highly disordered guest molecules. CCDC 1046717−1046719 contains the supplementary crystallographic data of **UTSA-74**, **UTSA-74a**, and **UTSA-74⊃$CO_2$**, respectively. These data can be obtained free of charge from the Cambridge Crystallographic Data Centre via www.ccdc.cam.ac.uk/data_request/cif.

## RESULTS AND DISCUSSION

**UTSA-74** was synthesized at a high temperature of 158 °C instead of 105 °C for the synthesis of Zn-MOF-74.[8a]The exact control of the solvent mixture ratio, particularly the water amount, is also necessary and important for getting high quality **UTSA-74**.

Single crystal X-ray diffraction reveals that **UTSA-74** crystallizes in rhombohedral, $R\bar{3}c$ space group and exhibits a three-dimensional porous framework with regular 1D channels along the *c* direction. There exist two crystallographically independent $Zn^{2+}$ sites. Zn1 site is four coordinated by two $dobdc^{4-}$ carboxylate oxygen atoms and two $dobdc^{4-}$ hydroxyl oxygen atoms, creating a tetrahedral geometry. Zn2 site shows six coordinated octahedral geometry, completed by four $dobdc^{4-}$ oxygen atoms (two carboxylate oxygen atoms plus two hydroxyl oxygen atoms) in the equatorial plane, and two terminal coordinated water molecules in the axis orientation (Figure 1a). Because these terminal water molecules can be possibly removed during thermal and/or vacuum activation, each of these Zn2 sites can presumably bind two gas molecules. Without consideration of these terminal solvent molecules, **UTSA-74** has an effective 1D aperture of about 8.0 Å, and the potential solvent-accessible volume of **UTSA-74** estimated by Platon program is 3474.9 $Å^3$ per unit cell volume 7272.9 $Å^3$, equal to 47.8% of the cell volume.[27]Compared with Zn-MOF-


DOI: 10.1021/jacs.6b02030
J. Am. Chem. Soc. 2016, 138, 5678−5684

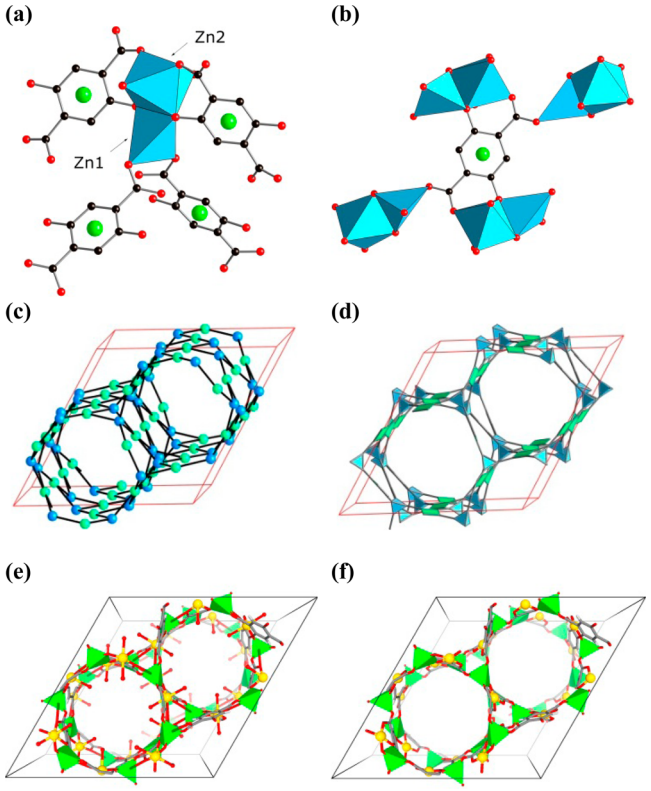


**Figure 1.** Single crystal X-ray structures of the as-synthesized **UTSA-74** indicating that (a) the binuclear $Zn_2(O)_2(CO_2)_4$ secondary building unit (one $Zn^{2+}$ is in a tetrahedral coordination while another one is in an octahedral coordination) acts as the four coordinated node, and (b) the organic linker $dobdc^{4-}$ acts as the second four coordinated node, to form (c and d) a three-dimensional framework of the novel **fgl** topology (the light blue ball and tetrahedron represent the $Zn_2(O)_2(CO_2)_4$ node while light green ball and square represent the $dobdc^{4-}$ node). (e) The highlighted octahedral Zn2 (yellow ball) is bound by two axial water molecules and (f) by the activated **UTSA-74a** in which two axial water molecules can be completely removed, generating accessible open Zn2 sites (yellow balls) which can potentially bind two gas molecules per metal center on the pore surfaces of the 1D channels of about 8.0 Å.

74 which has a 58.2% accessible pore space, **UTSA-74** has a slightly more condensed structure.

The purity of the bulk products was determined by comparison of the simulated and experimental PXRD patterns, and further supported by elemental analysis and thermogravimetric analysis. TGA reveals that the solvent molecules and coordinated water molecules can be removed by activating at 200 °C (see Supporting Information, Figures S1 and S2). **UTSA-74** can thus be easily activated at 200 °C under high vacuum to provide open metal sites on the pore surface channels of the resulting **UTSA-74a**, as evidenced by single crystal X-ray diffraction study (Figure 1f). The structure of **UTSA-74a** clearly indicates that each Zn2 potentially can bind two gas molecules. This is unusual in MOF structures, though it has been rarely revealed in porous M′MOFs from metalloligands.[26] The stability of **UTSA-74** is comparable to that of Zn-MOF-74, as shown in their PXRDs after immersion in water of variable pH values in the range 3−10 (Figure S3).

The permanent porosity of **UTSA-74a** was confirmed by $N_2$ adsorption at 77 K (Figure S4), exhibiting a fully reversible type-I isotherm. **UTSA-74a** has a BET surface area of 830 $m^2/g$ (Langmuir surface area of 996 $m^2/g$), a uniform pore size of 0.80 nm, and a total pore volume of 0.39 $cm^3/g$. Compared with Zn-MOF-74, **UTSA-74a** is less porous in terms of both pore volume and pore size, which matches with their corresponding structures.

We examined the $C_2H_2$ and $CO_2$ gas sorption isotherms of **UTSA-74a** at ambient temperature of 298 K and pressure of 100 kPa in order to figure out its potential for gas storage and separation. As expected, **UTSA-74a** takes up a large amount of $C_2H_2$ (145.0 $cm^3/cm^3$), which is comparable to 150 $cm^3/cm^3$ in Zn-MOF-74 (Figure 2).[15] However, to our big surprise,

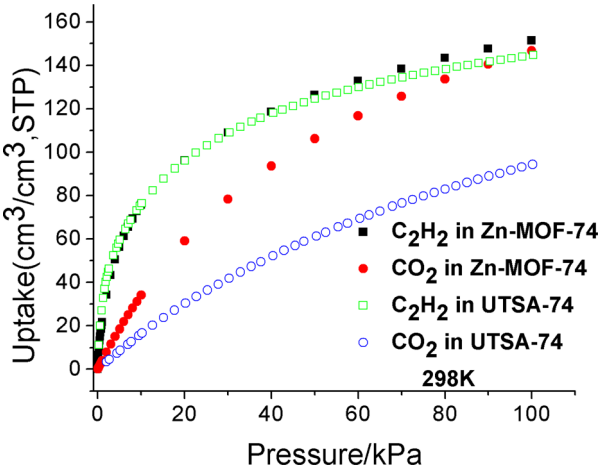


**Figure 2.** Comparison of sorption isotherms of $C_2H_2$ and $CO_2$ for **UTSA-74** and Zn-MOF-74 at 298 K.

**UTSA-74a** adsorbs a much smaller amount of $CO_2$ (95.0 $cm^3/cm^3$) than Zn-MOF-74 of 146 $cm^3/cm^3$, which is only about 2/3 of the $CO_2$ uptake in Zn-MOF-74.[14] This is really unusual.

In order to understand the unique sorption performance of **UTSA-74a** for $C_2H_2$ and $CO_2$, we performed detailed dispersion-corrected density-functional theory (DFT-D) calculations.[28] We found that the coordination configuration of the open $Zn^{2+}$ site is quite sensitive to gas adsorption. In the DFT-D optimized bare **UTSA-74a** structure, the open $Zn^{2+}$ and its four coordinating O are not in an ideal planar configuration, similar to what the experimental SXRD structure suggests. The slightly distorted $ZnO_4$ forms a pseudotetrahedral configuration, representing a natural way to minimize the coordination unsaturation of the $Zn^{2+}$ ion. Upon gas adsorption, the $ZnO_4$ in the optimized MOF structure becomes notably more planar, with Zn fully exposed on both sides of the $ZnO_4$ plane, and consequently, it maximizes its direct interactions with guest molecules (Figure 3a). For $C_2H_2$ adsorption in **UTSA-74a**, the calculation shows that the open Zn directly binds to C≡C (i.e., toward the acetylene molecule center), similar to $C_2H_2$ adsorption in Zn-MOF-74.[15] For a single $C_2H_2$ adsorption on the Zn site, the calculated static binding energy ($E_B$) is ∼43.9 kJ/mol, comparable to what was found in Zn-MOF-74 (∼43.8 kJ/mol, obtained using the same approach). Interestingly, when the metal sites are heavily populated, each pair of $C_2H_2$ molecules adsorbed on two neighboring open Zn sites in **UTSA-74a** are close to each other (with a H···C distance of ∼3.3 Å), leading to beneficial intermolecular interaction through $H^{\delta+}\cdots C^{\delta-}$ hydrogen bonding (Figure 3a). Consequently, the calculated average static adsorption energy of $C_2H_2$ increased notably to ∼49.0 kJ/


DOI: 10.1021/jacs.6b02030
J. Am. Chem. Soc. 2016, 138, 5678−5684

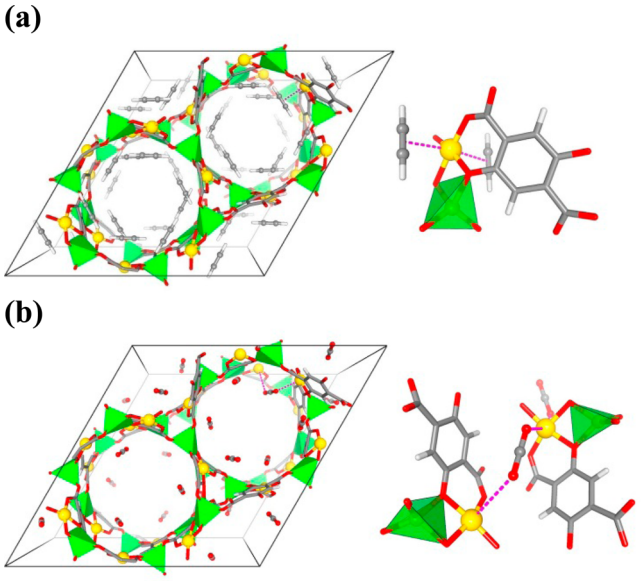


**Figure 3.** DFT-D optimized structure of (a) **UTSA-74⊃$C_2H_2$** and (b) X-ray single crystal structure of **UTSA-74⊃$CO_2$** in which the local coordination environments are shown on the right.

mol. For $CO_2$, the binding on the open-Zn in **UTSA-74a** is of a side-on fashion, similar to the case of $CO_2$ adsorption in Zn-MOF-74.[12] In our calculation, two possible adsorption configurations were considered. In the first configuration, each $CO_2$ binds to two neighboring open M sites simultaneously (Figure S5), and the DFT-D calculated static binding energy is ~33.4 kJ/mol. We expect that, at high $CO_2$ loading, the binding configuration may shift to one $CO_2$ per metal, which doubles the uptake when saturated, and maximizes the overall framework–guest interaction. In this case, the average $E_B$ decreases (by ~10%) to ~30.0 kJ/mol. This means that, at low $CO_2$ loading, the former configuration is energetically preferred, which is experimentally confirmed by the X-ray single crystal structure of **UTSA-74⊃$CO_2$** (Figure 3b). Overall, the $CO_2$ binding strength is comparable to what found in Zn-MOF-74 (~31.7 kJ/mol).

Our calculation results are fully consistent with the experimental results that the $C_2H_2$ adsorption capacity in **UTSA-74a** is nearly equal to the $C_2H_2$ adsorption capacity in Zn-MOF-74, as $C_2H_2$ adsorption is mainly determined by the open metal sites and the two structures have similar density of adsorptions sites on open metals. Furthermore, the calculation results also agree well with the experimental findings of a distinct adsorption amount for $C_2H_2$ and $CO_2$ in **UTSA-74a** at room temperature and 100 kPa ($n(C_2H_2)$:$n(CO_2)$ ~ 1.5), and a relatively smaller difference at 273 K and 100 kPa ($n(C_2H_2)$:$n(CO_2)$ ~ 1.2), as at room temperature the binding of a $CO_2$ molecule toward an open metal site adopts the first configuration of each $CO_2$ binding to two neighboring open M sites simultaneously, which results in moderate loading of $CO_2$, whereas at 273 K, the low temperature likely helps to shift the $CO_2$ binding toward the second configuration of one $CO_2$ per metal, which consequently increases the loading of $CO_2$. Moreover, on the basis of the calculation, the closest contacts between $C_2H_2$ molecules within the 1D channel is ~3.3 Å (H···C distance), indicative of a dense molecular packing after loading $C_2H_2$, whereas adjacent $CO_2$ molecules were largely separated by ca. 7.5 Å (O···O distance), indicative of a very loose packing after lower loading of $CO_2$. In contrast, in Zn-MOF-74,[12,15] the separation for both $C_2H_2$ and $CO_2$ molecules is comparable, such as $C_2H_2$ with a H···C distance of ~4.4 Å and $CO_2$ with a ~3.6 Å O···O distance. These results explain well the different $C_2H_2/CO_2$ selectivity between **UTSA-74a** and Zn-MOF-74.

Next, to evaluate the experimental adsorption energies of $C_2H_2$ and $CO_2$ in **UTSA-74a**, the calculation of isosteric heats of adsorption ($Q_{st}$), based on pure component isotherms of them at 298 and 273 K (Figure S6), is carried out using the Clausius–Clapeyron equation.[29] Figure 4a presents data on the

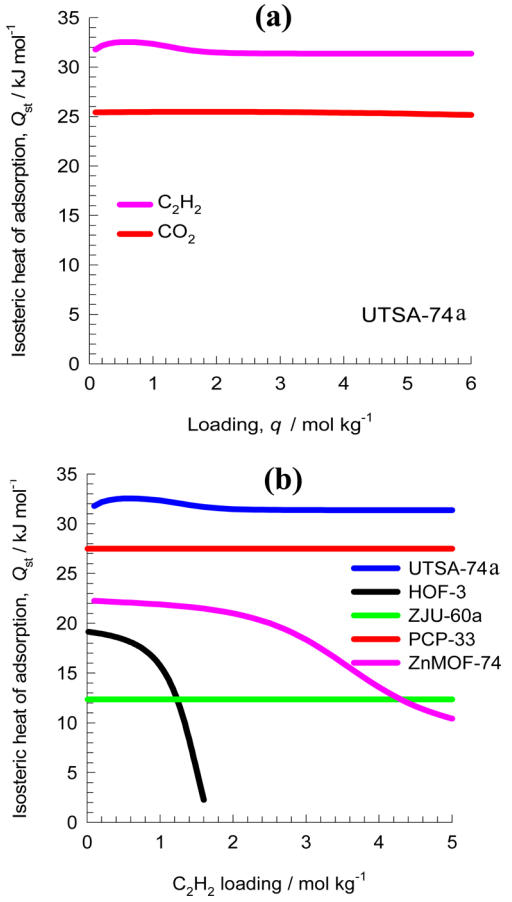


**Figure 4.** (a) Heats of adsorption of both $C_2H_2$ and $CO_2$ in **UTSA-74a** and (b) the comparison of the heats of adsorption of $C_2H_2$ among **UTSA-74a** and other MOFs.

loading dependence of $Q_{st}$ for $C_2H_2$ and $CO_2$. The obtained $Q_{st}$ value for $C_2H_2$ is above 31 kJ/mol, obviously bigger than that for $CO_2$ of 25 kJ/mol. The results agree well with observations that the guest–host interactions between $C_2H_2$ and **UTSA-74a** fairly exceed those between $CO_2$ and **UTSA-74a**. Moreover, the $Q_{st}$ value is also compared with other MOFs. The results is shown in Figure 4b, giving the hierarchy of **UTSA-74a** > PCP-33[30] > Zn-MOF-74[15] > ZJU-60a[31] ≈ HOF-3,[32] also indicative of superior affinity of **UTSA-74a** toward $C_2H_2$.

To obtain the potential in separation of $C_2H_2/CO_2$ by means of **UTSA-74a**, first, the commonly used approach upon the calculation by using the ideal adsorbed solution theory (IAST) is adopted.[33] As shown in Figure 5a, the simulated adsorption selectivity ($S_{ads}$) for the $C_2H_2/CO_2$ binary equimolar mixture is above 20 at low pressure, even far more than the best one previously established by HOF-3, but with the increase of


DOI: 10.1021/jacs.6b02030
J. Am. Chem. Soc. 2016, 138, 5678–5684

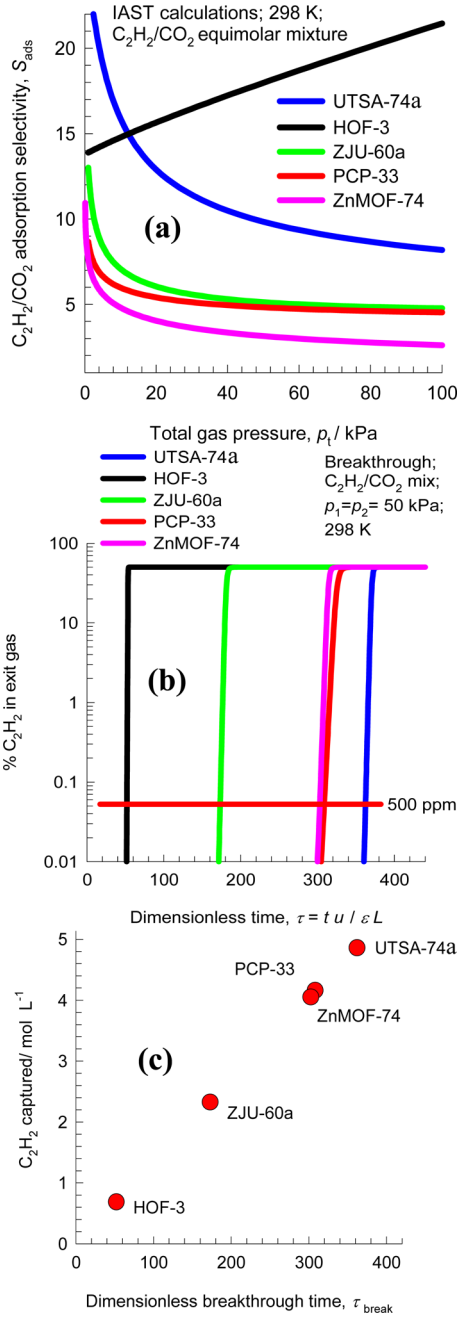


**Figure 5.** (a) IAST adsorption selectivities of $C_2H_2/CO_2$ in an equimolar mixture among **UTSA-74a** and other MOFs at 298 K. (b) Comparison of % $C_2H_2$ in the exit gas for beds packed with HOF-3, Zn-MOF-74, **UTSA-74a**, ZJU-60a, and PCP-33 plotted as a function of the dimensionless time. (c) Comparison of the moles of $C_2H_2$ captured per L of material during the interval for which the product gas is 99.95% $CO_2$, plotted as a function of the dimensionless breakthrough time, $\tau_{break}$.

pressure it gradually decreases down to 9 at 100 kPa. However, the $S_{ads}$ values at ambient pressure still fairly exceed those observed in other MOFs such as PCP-33, Zn-MOF-74, and ZJU-60a (less than 5). The results fully support the potential in a practical procedure for $C_2H_2/CO_2$ separation that in principle requires $S_{ads}$ greater than 8. The hierarchy of $S_{ads}$ values at 100 kPa is HOF-3 > **UTSA-74a** > ZJU-60a ≈ PCP-33 > Zn-MOF-74. Further, the performance of PSA units is also dictated by the uptake capacity. The component loading of $C_2H_2$, $q_1$, can be determined from IAST. The hierarchy of uptake capacities at 100 kPa, expressed as the number of moles of $C_2H_2$ adsorbed per L of adsorbent, is **UTSA-74a** > Zn-MOF-74 ≈ PCP-33 > ZJU-60a > HOF-3 (Figure S7), suggesting that the adsorption capacity of them would also determine the final separation performance of MOFs.

In order to properly evaluate the combined effects of selectivity and capacity, we carried out transient breakthrough simulations using the simulation methodology described in the literature.[30−33] The simulations in Figure S8 demonstrate the **UTSA-74a** is of potential use for this challenging separation of $C_2H_2/CO_2$ mixtures. During the initial transience, the effluent gas contains pure $CO_2$, and this continues until $C_2H_2$ starts breaking through because its uptake capacity in **UTSA-74a** has been reached. Figure 5b,c presents a comparison of $C_2H_2/CO_2$ separation performance with **UTSA-74a**, Zn-MOF-74, HOF-3, ZJU-60a, and PCP-33, resulting in the hierarchy HOF-3 < ZJU-60a < Zn-MOF-74 ≈ PCP-33 < **UTSA-74a**. On the other hand, we note that the amounts of $C_2H_2$ capture capacities have the following hierarchy: **UTSA-74a** > PCP-33 ≈ Zn-MOF-74 > ZJU-60a > HOF-3. Therefore, the excellent separation characteristics of **UTSA-74a** should be due to a combination of high selectivity (Figure 5a) and high $C_2H_2$ uptake capacity (Figure 2). The poor performance of HOF-3 is due to its low $C_2H_2$ uptake capacity (47 $cm^3/g$ at 296 K and 100 kPa), which further means that the low capacity cannot compensate for the high selectivity with this material.

To establish the $C_2H_2/CO_2$ separation performance of **UTSA-74** in practice, we also tested breakthrough experiments in which an equimolar $C_2H_2/CO_2$ mixture was flowed over a packed column of activated **UTSA-74a** solid with a total flow of 2 $cm^3$/min at 298 K. The result is shown in Figure 6, suggesting

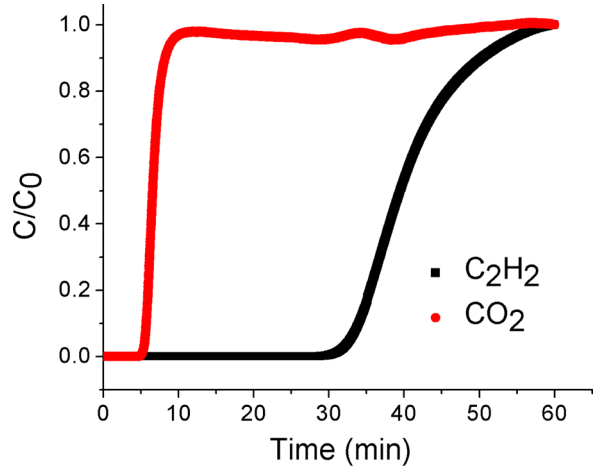


**Figure 6.** Experimental column breakthrough curve for an equimolar $C_2H_2/CO_2$ mixture (298 K, 1 bar) in an adsorber bed packed with **UTSA-74a**.

complete separation of $C_2H_2$ from the equimolar $C_2H_2/CO_2$ mixture by a column packed with activated **UTSA-74a** solid. As expected, the performance of **UTSA-74a** for $C_2H_2/CO_2$ separation is much more efficient than that of HOF-3, as clearly demonstrated in their separation factors of 20.1 and 2.04, respectively, determined through experimental breakthrough. To the best of our knowledge, **UTSA-74a** is also the first example of porous MOFs whose separation of the $C_2H_2/CO_2$ mixture has been clearly established by experimental


DOI: 10.1021/jacs.6b02030
J. Am. Chem. Soc. 2016, 138, 5678−5684

breakthrough.[34] It is worth emphasizing that the $C_2H_2/CO_2$ separation is a very challenging one given the fact that these two gas molecules have very similar shapes, dimensions (332 × 334 × 570 $pm^3$ versus 318.9 × 333.9 × 536.1 $pm^3$), and boiling points (−84 °C versus −78.5 °C). Such a separation is essential to get a high purity of acetylene for its commercial usage.[35]

## CONCLUSION

In conclusion, we have realized a new porous metal−organic framework **UTSA-74** from the well-explored organic linker $H_4$dobdc = 2,5-dioxido-1,4-benzenedicarboxylic acid at higher reaction temperature. **UTSA-74** is the structure isomer of the well-known Zn-MOF-74, and both of them have high thermostability and robustness, and are characteristic of one-dimensional channels of about 11 and 8 Å, respectively, with high densities of open metal sites immobilized on their pore surfaces. These similar basic structural characteristics might indicate that **UTSA-74** will become another promising prototypical MOF for diverse applications, because we in principle can incorporate different types of metal ions such as $Mg^{2+}$, $Ni^{2+}$, $Co^{2+}$, $Mn^{2+}$, $Fe^{2+}$, and $Cu^{2+}$ into the isostructural MOFs and postfunctionalize the pores for their molecular recognition and chemical transformations. **UTSA-74a** has a slightly higher volumetric open metal site density (8.25 mmol/$cm^3$) than MOF-74 (7.50 mmol/$cm^3$) and also unique open metal sites which can bind two gas molecules per metal center, which differentiates itself from the well-known MOF-74. The significantly enhanced performance for the $C_2H_2/CO_2$ separations, as demonstrated in this work, is the first example of the promising applications of this new series of MOF materials. It is expected that more isostructural MOFs of **UTSA-74** will be emerging in the near future for their variety of applications. From a structure point of view, the generation of two accessible open metal sites per metal center within porous MOFs is unusual. The existence of octahedral metal sites with two terminal solvent molecules within a MOF is the prerequisite;[36] more importantly, such metal sites need to be stabilized through their bondage with other metal sites through the formation of metal-cluster based secondary building units and their assembly into a robust framework structure. Further exploration on MOFs might lead to more porous MOFs with such special accessible metal sites and pore structures for their diverse applications.

## ASSOCIATED CONTENT

### Supporting Information

The Supporting Information is available free of charge on the ACS Publications website at DOI: 10.1021/jacs.6b02030.

Crystallographic data, TG, PXRD, $N_2$ adsorption isotherm, density functional theory calculations, dual Langmuir−Freundlich isotherm model fitting, isosteric heat of adsorption calculation, IAST calculations of adsorption selectivities, transient breakthrough simulations, and column breakthrough test setup with procedures and measurements (PDF)

Crystallographic data for **UTSA-74** (CIF)

Crystallographic data for **UTSA-74a** (CIF)

Crystallographic data for **UTSA-74⊃$CO_2$** (CIF)

## AUTHOR INFORMATION

### Corresponding Author

*banglin.chen@utsa.edu

### Notes

The authors declare no competing financial interest.

## ACKNOWLEDGMENTS

This work was supported by the NSF of China (21203022, 21261001, 21361001), the Natural Science Foundation of Jiangxi Province of China (no. 20143ACB20002), the Young Scientist Training Program of Jiangxi Province of China (no. 20142BCB23018), KAUST for the Competitive Research Funds (FCC/1/1972-02-01), and the Welch Foundation (AX-1730).

## REFERENCES

(1) (a) Furukawa, H.; Cordova, K. E.; O'Keeffe, M.; Yaghi, O. M. *Science* **2013**, *341*, 974. (b) Kitagawa, S.; Kitaura, R.; Noro, S. *Angew. Chem., Int. Ed.* **2004**, *43*, 2334. (c) Wang, C.; Liu, D. M.; Lin, W. B. *J. Am. Chem. Soc.* **2013**, *135*, 13222. (d) Chen, B.; Xiang, S. C.; Qian, G. D. *Acc. Chem. Res.* **2010**, *43*, 1115. (e) Cui, Y. J.; Li, B.; He, H. J.; Zhou, W.; Chen, B.; Qian, G. D. *Acc. Chem. Res.* **2016**, *49*, 483.

(2) (a) Zhou, H. C.; Long, J. R.; Yaghi, O. M. *Chem. Rev.* **2012**, *112*, 673. (b) Zhou, H. C.; Kitagawa, S. *Chem. Soc. Rev.* **2014**, *43*, 5415.

(3) (a) Hu, Z. C.; Lustig, W. P.; Zhang, J. M.; Zheng, C.; Wang, H.; Teat, S. J.; Gong, Q. H.; Rudd, N. D.; Li, J. *J. Am. Chem. Soc.* **2015**, *137*, 16209. (b) Nijem, N.; Wu, H. H.; Canepa, P.; Marti, A.; Balkus, K. J., Jr.; Thonhauser, T.; Li, J.; Chabal, Y. J. *J. Am. Chem. Soc.* **2012**, *134*, 15201. (c) Zhang, J. P.; Chen, X. M. *J. Am. Chem. Soc.* **2009**, *131*, 5516. (d) Liao, P. Q.; Chen, H. Y.; Zhou, D. D.; Liu, S. Y.; He, C. T.; Rui, Z. B.; Ji, H. B.; Zhang, J. P.; Chen, X. M. *Energy Environ. Sci.* **2015**, *8*, 1011. (e) Yang, Q. H.; Xu, Q.; Yu, S. H.; Jiang, H. L. *Angew. Chem., Int. Ed.* **2016**, *55*, 3685.

(4) (a) Zhu, Q.; Li, J.; Xu, Q. *J. Am. Chem. Soc.* **2013**, *135*, 10210. (b) Wang, K. C.; Lv, X. L.; Feng, D. W.; Li, J.; Chen, S. M.; Sun, J. L.; Song, L.; Xie, Y. B.; Li, J. R.; Zhou, H. C. *J. Am. Chem. Soc.* **2016**, *138*, 914. (c) Li, B. Y.; Leng, K. Y.; Zhang, Y. M.; Dynes, J. J.; Wang, J.; Hu, Y. F.; Ma, D. X.; Shi, Z.; Zhu, L. K.; Zhang, D. L.; Sun, Y. Y.; Chrzanowski, M.; Ma, S. Q. *J. Am. Chem. Soc.* **2015**, *137*, 4243. (d) Lin, Q. P.; Bu, X. H.; Kong, A.; Mao, C. Y.; Zhao, X.; Bu, F.; Feng, P. Y. *J. Am. Chem. Soc.* **2015**, *137*, 2235. (e) Zhang, S. Y.; Wojtas, L.; Zaworotko, M. J. *J. Am. Chem. Soc.* **2015**, *137*, 12045. (f) Liu, C.; Luo, T. Y.; Feura, E. S.; Zhang, C.; Rosi, N. L. *J. Am. Chem. Soc.* **2015**, *137*, 10508. (g) Ramaswamy, P.; Wong, N. E.; Gelfand, B. S.; Shimizu, G. K. *J. Am. Chem. Soc.* **2015**, *137*, 7640. (h) Howarth, A. J.; Katz, M. J.; Wang, T. C.; Platero-Prats, A. E.; Chapman, K. W.; Hupp, J. T.; Farha, O. K. *J. Am. Chem. Soc.* **2015**, *137*, 7488. (i) Xue, D. X.; Belmabkhout, Y.; Shekhah, O.; Jiang, H.; Adil, K.; Cairns, A. J.; Eddaoudi, M. *J. Am. Chem. Soc.* **2015**, *137*, 5034. (j) Yang, S. H.; Ramirez-Cuesta, A. J.; Newby, R.; Garcia-Sakai, V.; Manuel, P.; Callear, S. K.; Campbell, S. I.; Tang, C. C.; Schröder, M. *Nat. Chem.* **2014**, *7*, 121. (k) Stoeck, U.; Nickerl, G.; Burkhardt, U.; Senkovska, I.; Kaskel, S. *J. Am. Chem. Soc.* **2012**, *134*, 17335.

(5) Li, H.; Eddaoudi, M.; O'Keeffe, M.; Yaghi, O. M. *Nature* **1999**, *402*, 276.

(6) Chui, S. S. Y.; Lo, S. M. F.; Charmant, J. P. H.; Orpen, A. G.; Williams, I. D. *Science* **1999**, *283*, 1148.

(7) (a) Subramanian, S.; Zaworotko, M. J. *Angew. Chem., Int. Ed. Engl.* **1995**, *34*, 2561. (b) Noro, S.; Kitagawa, S.; Kondo, M.; Seki, K. *Angew. Chem., Int. Ed.* **2000**, *39*, 2081. (c) Nugent, P.; Belmabkhout, Y.; Burd, S. D.; Cairns, A. J.; Luebke, R.; Forrest, K.; Pham, T.; Ma, S. Q.; Space, B.; Wojtas, L.; Eddaoudi, M.; Zaworotko, M. J. *Nature* **2013**, *495*, 80.

(8) (a) Rosi, N. L.; Kim, J.; Eddaoudi, M.; Chen, B.; O'Keeffe, M.; Yaghi, O. M. *J. Am. Chem. Soc.* **2005**, *127*, 1504. (b) Dietzel, P. D. C.; Morita, Y.; Blom, R.; Fjellvag, H. *Angew. Chem., Int. Ed.* **2005**, *44*, 6354. (c) Dietzel, P. D. C.; Panella, B.; Hirscher, M.; Blom, R.; Fjellvag, H. *Chem. Commun.* **2006**, 959. (d) Vitillo, J. G.; Regli, L.; Chavan, S.; Ricchiardi, G.; Spoto, G.; Dietzel, P. D. C.; Bordiga, S.; Zecchina, A. *J. Am. Chem. Soc.* **2008**, *130*, 8386. (e) Dietzel, P. D. C.; Johnsen, R. E.; Blom, R.; Fjellvag, H. *Chem. - Eur. J.* **2008**, *14*, 2389.



DOI: 10.1021/jacs.6b02030
*J. Am. Chem. Soc.* 2016, 138, 5678−5684

(f) Dietzel, P. D. C.; Johnsen, R. E.; Fjellvag, H.; Bordiga, S.; Groppo, E.; Chavan, S.; Blom, R. *Chem. Commun.* **2008**, 5125.
(9) (a) Park, K. S.; Ni, Z.; Côté, A. P.; Choi, J. Y.; Huang, R.; Uribe-Romo, F. J.; Chae, H. K.; O'Keeffe, M.; Yaghi, O. M. *Proc. Natl. Acad. Sci. U. S. A.* **2006**, *103*, 10186. (b) Huang, X. C.; Lin, Y. Y.; Zhang, J. P.; Chen, X. M. *Angew. Chem., Int. Ed.* **2006**, *45*, 1557.
(10) Férey, G.; Mellot-Draznieks, C.; Serre, C.; Millange, F.; Dutour, J.; Surblé, S.; Margiolaki, I. *Science* **2005**, *309*, 2040.
(11) Cavka, J. H.; Jakobsen, S.; Olsbye, U.; Guillou, N.; Lamberti, C.; Bordiga, S.; Lillerud, K. P. *J. Am. Chem. Soc.* **2008**, *130*, 13850.
(12) (a) Zhou, W.; Wu, H.; Yildirim, T. *J. Am. Chem. Soc.* **2008**, *130*, 15268. (b) Vitillo, J. G.; Regli, L.; Chavan, S.; Ricchiardi, G.; Spoto, G.; Dietzel, P. D. C.; Bordiga, S.; Zecchina, A. *J. Am. Chem. Soc.* **2008**, *130*, 8386. (c) Queen, W. L.; Hudson, M. R.; Bloch, E. D.; Mason, J. A.; Gonzalez, M.; Lee, J. S.; Gygi, D.; Howe, J. D.; Lee, K.; Darwish, T. A.; James, M.; Peterson, V. K.; Teat, S. J.; Smit, B.; Neaton, J. B.; Long, J. R.; Brown, C. M. *Chem. Sci.* **2014**, *5*, 4569.
(13) (a) Nijem, N.; Kong, L. Z.; Zhao, Y. G.; Wu, H. H.; Li, J.; Langreth, D. C.; Chabal, Y. J. *J. Am. Chem. Soc.* **2011**, *133*, 4782. (b) Wang, L. J.; Deng, H. X.; Furukawa, H.; Gándara, F.; Cordova, K. E.; Peri, D.; Yaghi, O. M. *Inorg. Chem.* **2014**, *53*, 5881. (c) Valvekens, P.; Vandichel, M.; Waroquier, M.; Speybroeck, V. V.; Vos, D. D. *J. Catal.* **2014**, *317*, 1.
(14) (a) Caskey, S. R.; Wong-Foy, A. G.; Matzger, A. J. *J. Am. Chem. Soc.* **2008**, *130*, 10870. (b) Britt, D.; Furukawa, H.; Wang, B.; Glover, T. G.; Yaghi, O. M. *Proc. Natl. Acad. Sci. U. S. A.* **2009**, *106*, 20637. (c) Kong, X. Q.; Scott, E.; Ding, W.; Mason, J. A.; Long, J. R.; Reimer, J. A. *J. Am. Chem. Soc.* **2012**, *134*, 14341.
(15) Xiang, S. C.; Zhou, W.; Zhang, Z. J.; Green, M. A.; Liu, Y.; Chen, B. L. *Angew. Chem., Int. Ed.* **2010**, *49*, 4615.
(16) Wu, H.; Zhou, W.; Yildirim, T. *J. Am. Chem. Soc.* **2009**, *131*, 4995.
(17) (a) Bloch, E. D.; Queen, W. L.; Krishna, R.; Zadrozny, J. M.; Brown, C. M.; Long, J. R. *Science* **2012**, *335*, 1606. (b) He, Y. B.; Krishna, R.; Chen, B. L. *Energy Environ. Sci.* **2012**, *5*, 9107.
(18) Bloch, E. D.; Murray, L. J.; Queen, W. L.; Chavan, S.; Maximoff, S. N.; Bigi, J. P.; Krishna, R.; Peterson, V. K.; Grandjean, F.; Long, G. J.; Smit, B.; Bordiga, S.; Brown, C. M.; Long, J. R. *J. Am. Chem. Soc.* **2011**, *133*, 14814.
(19) Bloch, E. D.; Hudson, M. R.; Mason, J. A.; Chavan, S.; Crocellà, V.; Howe, J. D.; Lee, K.; Dzubak, A. L.; Queen, W. L.; Zadrozny, J. M.; Geier, S. J.; Lin, L. C.; Gagliardi, L.; Smit, B.; Neaton, J. B.; Bordiga, S.; Brown, C. M.; Long, J. R. *J. Am. Chem. Soc.* **2014**, *136*, 10752.
(20) Xiao, D. J.; Bloch, E. D.; Mason, J. A.; Queen, W. L.; Hudson, M. R.; Planas, N.; Borycz, J.; Dzubak, A. L.; Verma, P.; Lee, K.; Bonino, F.; Crocellà, V.; Yano, J.; Bordiga, S.; Truhlar, D. G.; Gagliardi, L.; Brown, C. M.; Long, J. R. *Nat. Chem.* **2014**, *6*, 590.
(21) Bloch, E. D.; Queen, W. L.; Chavan, S.; Wheatley, P. S.; Zadrozny, J. M.; Morris, R.; Brown, C. M.; Lamberti, C.; Bordiga, S.; Long, J. R. *J. Am. Chem. Soc.* **2015**, *137*, 3466.
(22) Cho, H. S.; Deng, H. X.; Miyasaka, K.; Dong, Z. Y.; Cho, M.; Neimark, A. V.; Kang, J. K.; Yaghi, O. M.; Terasaki, O. M. *Nature* **2015**, *527*, 503.
(23) (a) McDonald, T. M.; Lee, W. R.; Mason, J. A.; Wiers, B. M.; Hong, C. S.; Long, J. R. *J. Am. Chem. Soc.* **2012**, *134*, 7056. (b) McDonald, T. M.; Mason, J. A.; Kong, X. Q.; Bloch, E. D.; Gygi, D.; Dani, A.; Crocellà, V.; Giordanino, F.; Odoh, S. O.; Drisdell, W. S.; Vlaisavljevich, B.; Dzubak, A. L.; Poloni, R.; Schnell, S. K.; Planas, N.; Lee, K.; Pascal, T.; Wan, L. F.; Prendergast, D.; Neaton, J. B.; Smit, B.; Kortright, J. B.; Gagliardi, L.; Bordiga, S.; Reimer, J. A.; Long, J. R. *Nature* **2015**, *519*, 303.
(24) Deng, H. X.; Grunder, S.; Cordova, K. E.; Valente, C.; Furukawa, H.; Hmadeh, M.; Gándara, F.; Whalley, A. C.; Liu, Z.; Asahina, S.; Kazumori, H.; O'Keeffe, M.; Terasaki, O.; Stoddart, J. F.; Yaghi, O. M. *Science* **2012**, *336*, 1018.
(25) Hu, T. L.; Wang, H. L.; Li, B.; Krishna, R.; Wu, H.; Zhou, W.; Zhao, Y. F.; Han, Y.; Wang, X.; Zhu, W. D.; Yao, Z. Z.; Xiang, S. C.; Chen, B. *Nat. Commun.* **2015**, *6*, 7328.
(26) (a) Chen, B.; Zhao, X.; Putkham, A.; Hong, K.; Lobkovsky, E. B.; Hurtado, E. J.; Fletcher, A. J.; Thomas, K. M. *J. Am. Chem. Soc.* **2008**, *130*, 6411. (b) Xiang, S. C.; Zhang, Z. J.; Zhao, C. G.; Hong, K. L.; Zhao, X. B.; Ding, D. R.; Xie, M. H.; Wu, C. D.; Das, M. C.; Gill, R.; Thomas, K. M.; Chen, B. *Nat. Commun.* **2011**, *2*, 204. (c) Das, M. C.; Xiang, S.; Zhang, Z.; Chen, B. *Angew. Chem., Int. Ed.* **2011**, *50*, 10510.
(27) Spek, A. L. *PLATON*; 2001.
(28) Giannozzi, P.; Baroni, S.; Bonini, N.; Calandra, M.; Car, R.; Cavazzoni, C.; Ceresoli, D.; Chiarotti, G. L.; Cococcioni, M.; Dabo, I.; Dal Corso, A.; Fabris, S.; Fratesi, G.; de Gironcoli, S.; Gebauer, R.; Gerstmann, U.; Gougoussis, C.; Kokalj, A.; Lazzeri, M.; Martin-Samos, L.; Marzari, N.; Mauri, F.; Mazzarello, R.; Paolini, S.; Pasquarello, A.; Paulatto, L.; Sbraccia, C.; Scandolo, S.; Sclauzero, G.; Seitsonen, A. P.; Smogunov, A.; Umari, P.; Wentzcovitch, R. M. *J. Phys.: Condens. Matter* **2009**, *21*, 395502.
(29) (a) Dincă, M.; Long, J. R. *J. Am. Chem. Soc.* **2005**, *127*, 9376. (b) Yang, S.; Lin, X.; Blake, A. J.; Walker, G. S.; Hubberstey, P.; Champness, N. R.; Schröder, M. *Nat. Chem.* **2009**, *1*, 487.
(30) Duan, J.; Jin, W.; Krishna, R. *Inorg. Chem.* **2015**, *54*, 4279.
(31) Duan, X.; Zhang, Q.; Cai, J.; Yang, Y.; Cui, Y.; He, Y.; Wu, C.; Krishna, R.; Chen, B.; Qian, G. *J. Mater. Chem. A* **2014**, *2*, 2628.
(32) Li, P.; He, Y. B.; Zhao, Y. F.; Weng, L. H.; Wang, H. L.; Krishna, R.; Wu, H.; Zhou, W.; O'Keeffe, M.; Han, Y.; Chen, B. *Angew. Chem., Int. Ed.* **2015**, *54*, 574.
(33) (a) Myers, A. L.; Prausnitz, J. M. *AIChE J.* **1965**, *11*, 121. (b) Krishna, R.; Long, J. R. *J. Phys. Chem. C* **2011**, *115*, 12941. (c) Krishna, R. *Microporous Mesoporous Mater.* **2014**, *185*, 30. (d) Krishna, R.; Baur, R. *Sep. Purif. Technol.* **2003**, *33*, 213.
(34) (a) Matsuda, R.; Kitaura, R.; Kitagawa, S.; Kubota, Y.; Belosludov, R. V.; Kobayashi, T. C.; Sakamoto, H.; Chiba, T.; Takata, M.; Kawazoe, Y.; Mita, Y. *Nature* **2005**, *436*, 238. (b) He, Y.; Xiang, S.; Zhang, Z.; Xiong, S.; Fronczek, F. R.; Krishna, R.; O'Keeffe, M.; Chen, B. *Chem. Commun.* **2012**, *48*, 10856. (c) Xu, H.; He, Y.; Zhang, Z.; Xiang, S.; Cai, J.; Cui, Y.; Yang, Y.; Qian, G.; Chen, B. *J. Mater. Chem. A* **2013**, *1*, 77. (d) Eguchi, R.; Uchida, S.; Mizuno, N. *Angew. Chem., Int. Ed.* **2012**, *51*, 1635. (e) Foo, M. L.; Matsuda, R.; Hijikata, Y.; Krishna, R.; Sato, H.; Horike, S.; Hori, A.; Duan, J. G.; Sato, Y.; Kubota, Y.; Takata, M.; Kitagawa, S. *J. Am. Chem. Soc.* **2016**, *138*, 3022.
(35) Zhang, Z.; Xiang, S.; Chen, B. *CrystEngComm* **2011**, *13*, 5983.
(36) Stein, I.; Ruschewitz, U. *Acta Crystallogr., Sect. E: Struct. Rep. Online* **2005**, *E61*, m2680.


DOI: 10.1021/jacs.6b02030
*J. Am. Chem. Soc.* 2016, 138, 5678−5684

# UTSA-74: An Isomeric MOF-74 with Two Accessible Binding Sites *per* Metal Center for Highly Selective Gas Separation

Feng Luo, Changsheng Yan, Lilong Dang, Rajamani Krishna, Wei Zhou, Xinglong Dong, Yu Han, Tong-Liang Hu, Michael O'Keeffe, Lingling Wang, Mingbiao Luo, Rui-Biao Lin, Banglin Chen*

**Table S1.** Crystallographic data of **UTSA-74**, **UTSA-74a**, and **UTSA-74⊃$CO_2$**.

| Compounds | **UTSA-74** | **UTSA-74a** | **UTSA-74⊃$CO_2$** |
|---|---|---|---|
| Empirical formula | $C_{24}H_{12}O_{21}Zn_6$ | $C_{24}H_6O_{18}Zn_6$ | $C_{27}H_6O_{24}Zn_6$ |
| Formula weight | 1028.79 | 974.51 | 1106.54 |
| Temperature (K) | 296(2) | 296(2) | 120(2) |
| Wavelength (Å) | 0.71073 | 0.71073 | 0.71073 |
| Crystal system, space group | Rhombohedral, R-3c | Rhombohedral, R-3c | Rhombohedral, R-3c |
| Unit cell dimensions (Å) | a=b=22.9170(4), c=15.9024(5) | a=b=22.9556(13), c=15.883(2) | a=b=22.9511(8), c=15.8965(11) |
| Volume ($Å^3$) | 7232.8(3) | 7248.2(12) | 7251.7(6) |
| Z, Calculated density ($Mg/m^3$) | 12， 1.409 | 6， 1.34 | 6， 1.52 |
| F(000) | 2988 | 2844 | 3240 |
| Crystal size (mm) | 0.18×0.08×0.08 | 0.18×0.08×0.08 | 0.18×0.08×0.08 |
| Theta range for data collection | 2.76-27.51 | 2.76-26.00 | 2.42-27.64 |
| Completeness to theta | 99.6% | 99.6% | 97.3% |
| GOF | 1.215 | 0.915 | 1.282 |
| Final R indices [I>2sigma(I)] | $R_1$=0.0772, ω$R_2$=0.1717 | $R_1$=0.1221, ω$R_2$=0.2445 | $R_1$=0.1631, ω$R_2$=0.3024 |

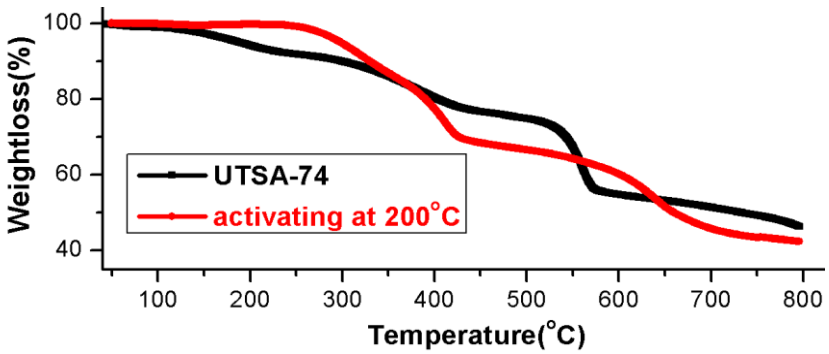


**Figure S1.** The TG plots of as-synthesized samples and activated samples of **UTSA-74.**

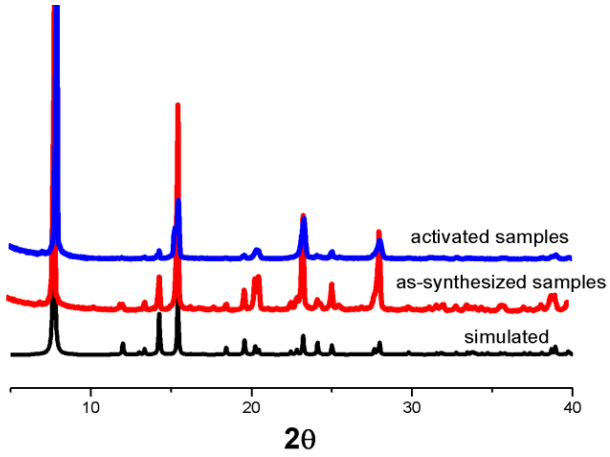


**Figure S2.** The PXRD patterns of as-synthesized and activated samples of **UTSA-74**, as well as the simulated PXRD patterns calculated from the single crystal data of **UTSA-74**.

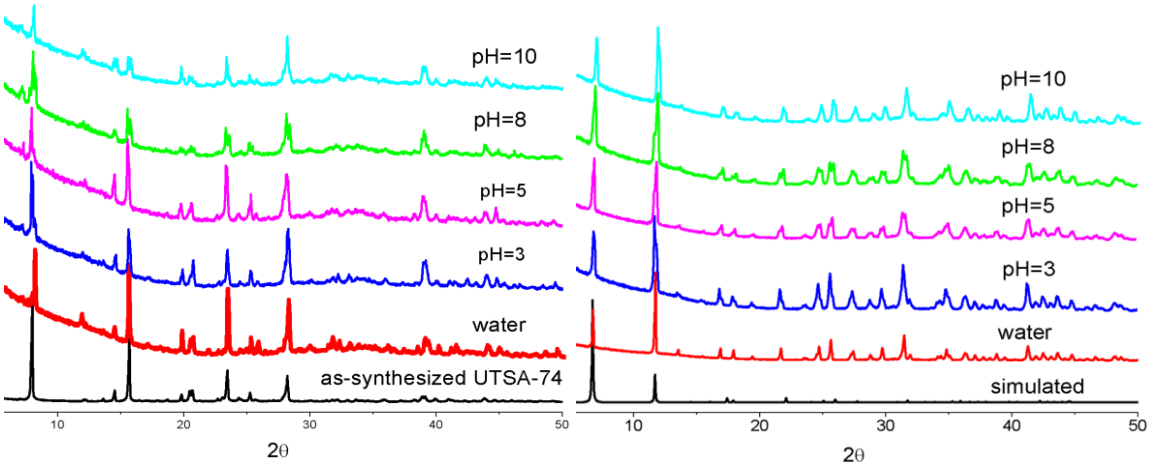


**Figure S3.** The PXRD patterns of **UTSA-74** and Zn-MOF-74 after immerging in water with the pH values in the range of 3 to 10 for 24 h, respectively (**UTSA-74** (left); Zn-MOF-74 (right)).

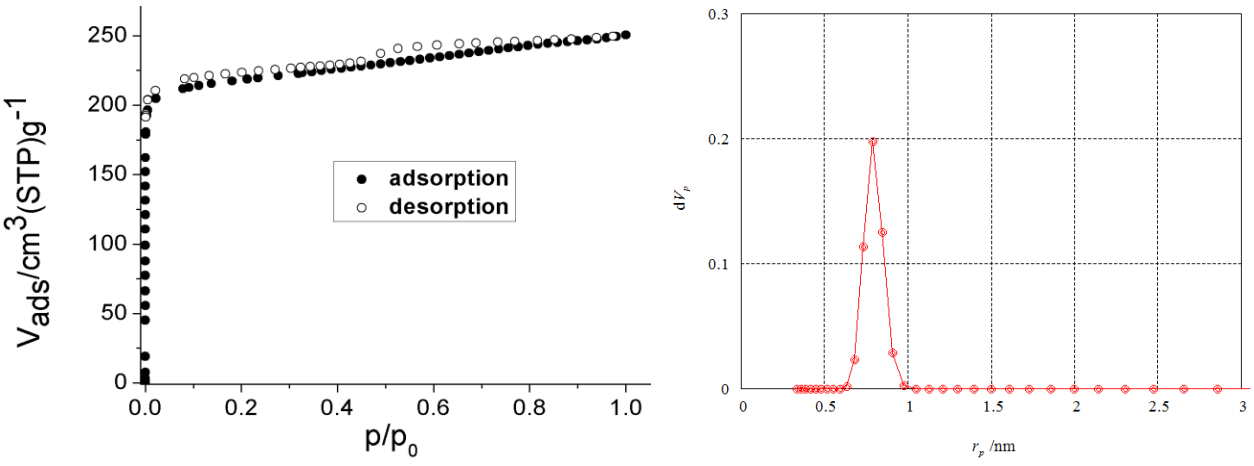


**Figure S4.** The $N_2$ adsorption isotherms at 77K and the pore distribution of **UTSA-74a**.

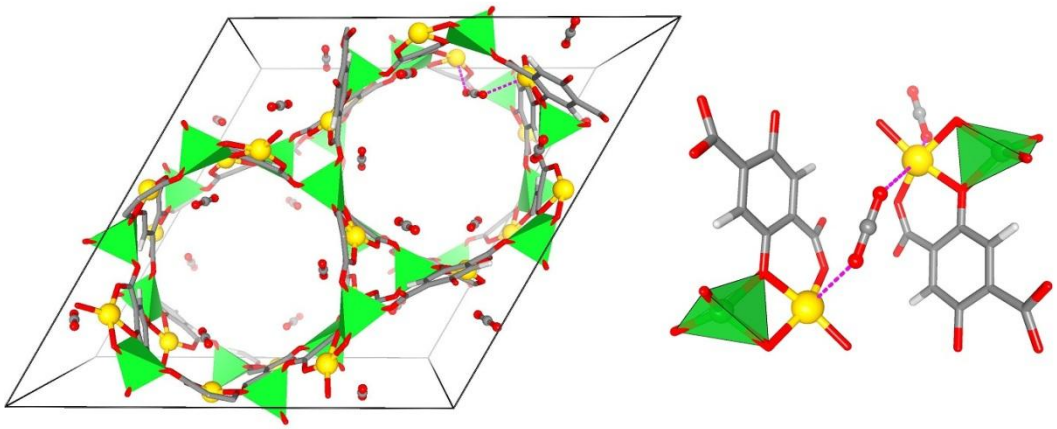

**Figure S5.** The DFT-D optimized structure of **UTSA-74⊃$CO_2$** in which the local coordination environments are shown at the right.

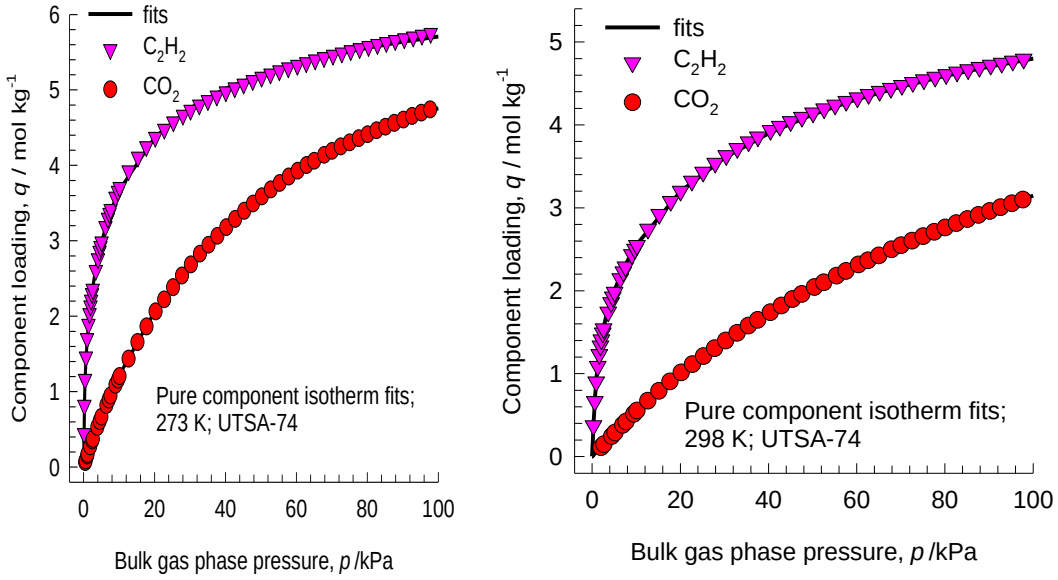


**Figure S6.** Comparison of absolute component loadings for $C_2H_2$, and $CO_2$ at (a) 273 K, and (b) 298 K in UTSA-74a with the isotherm fits. The experimentally measured excess loadings for $C_2H_2$, and $CO_2$ at temperatures of 273 K, and 298 K in UTSA-74a were fitted with the dual-Langmuir-Freundlich isotherm model

$$q = q_{A,sat}\frac{b_A p^{\nu_A}}{1+b_A p^{\nu_A}} + q_{B,sat}\frac{b_B p^{\nu_B}}{1+b_B p^{\nu_B}} \tag{1}$$

with $T$-dependent parameters $b_A$, and $b_B$

$$b_A = b_{A0}\exp\left(\frac{E_A}{RT}\right); \quad b_B = b_{B0}\exp\left(\frac{E_B}{RT}\right) \tag{2}$$

The parameters are provided in Table S2.

**Table S2.** Dual-Langmuir-Freundlich parameter fits for $C_2H_2$, and $CO_2$ in **UTSA-74a**.

| | Site A | | | | Site B | | | |
|---|---|---|---|---|---|---|---|---|
| | $q_{A,sat}$ mol kg$^{-1}$ | $b_{A0}$ | $E_A$ kJ mol$^{-1}$ | $\nu_A$ dimensionless | $q_{B,sat}$ mol kg$^{-1}$ | $b_{B0}$ | $E_B$ kJ mol$^{-1}$ | $\nu_B$ dimensionless |

| | | $Pa^{-\nu_i}$ | | | | $Pa^{-\nu_i}$ | | |
|---|---|---|---|---|---|---|---|---|
| $C_2H_2$ | 0.7 | $1.81\times10^{-16}$ | 60.2 | 1.8 | 6.2 | $2.30\times10^{-7}$ | 20.7 | 0.66 |
| $CO_2$ | 4.8 | $2.02\times10^{-12}$ | 37 | 1 | 2.4 | $5.37\times10^{-6}$ | 2 | 1 |

**Isosteric heat of adsorption.**

The binding energies of $C_2H_2$, and $CO_2$ in **UTSA-74a** are reflected in the isosteric heat of adsorption, $Q_{st}$, defined as

$$Q_{st} = RT^2\left(\frac{\partial \ln p}{\partial T}\right)_q \tag{3}$$

These values were determined using the pure component isotherm fits.

**IAST calculations of adsorption selectivities.**

In order to establish the feasibility of $C_2H_2/CO_2$ separations we performed calculations using the Ideal Adsorbed Solution Theory (IAST) of Myers and Prausnitz.

Let us determine the adsorption selectivity, $S_{ads}$, defined for separation of a binary mixture of species $i$ and $j$ by

$$S_{ads} = \frac{q_i/q_j}{p_i/p_j} \tag{4}$$

where the $q_i$ represent the molar loadings of component $i$ that is in equilibrium with a bulk gas phase with partial pressures $p_i$ in the mixture.

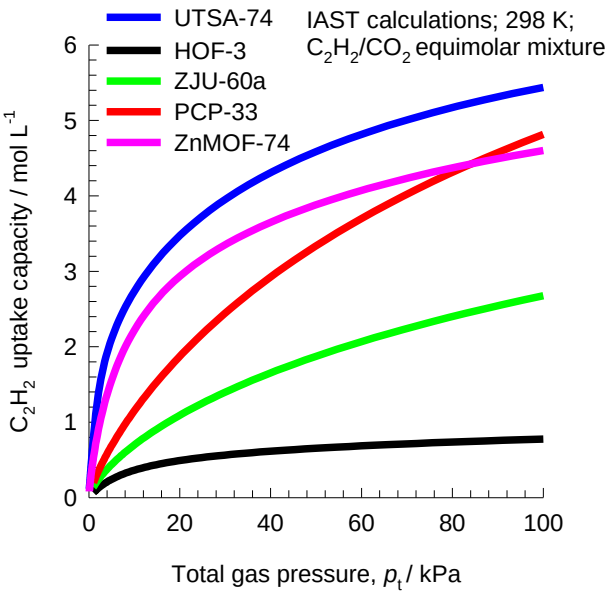


**Figure S7.** IAST calculations of uptake capacity of $C_2H_2$, for separation of 50/50 $C_2H_2/CO_2$ mixture at 298 K using HOF-3, **UTSA-74a**, ZJU-60a, and PCP-33.

**Transient breakthrough simulations.**

The performance of industrial fixed bed adsorbers is dictated by a combination of adsorption selectivity and uptake capacity. For a proper comparison of various MOFs, we perform transient breakthrough simulations using the simulation methodology described in the literature. For the breakthrough simulations, the following parameter values were used: length of packed bed, $L$ = 0.3 m; voidage of packed bed, $\varepsilon$= 0.4; superficial gas velocity at inlet, $u$ = 0.04 m/s. The framework density of **UTSA-74a** is 1401 kg $m^{-3}$. The breakthrough time, $\tau_{break}$, is define as the time at which the exit gas contains < 0.05% = 500 ppm $C_2H_2$. The amount of $C_2H_2$ captured during the time interval 0-$\tau_{break}$ can be determined from a material balance. These amounts, expressed as moles $C_2H_2$

captured per L of framework material, are plotted against $\tau_{break}$ in Table S3.

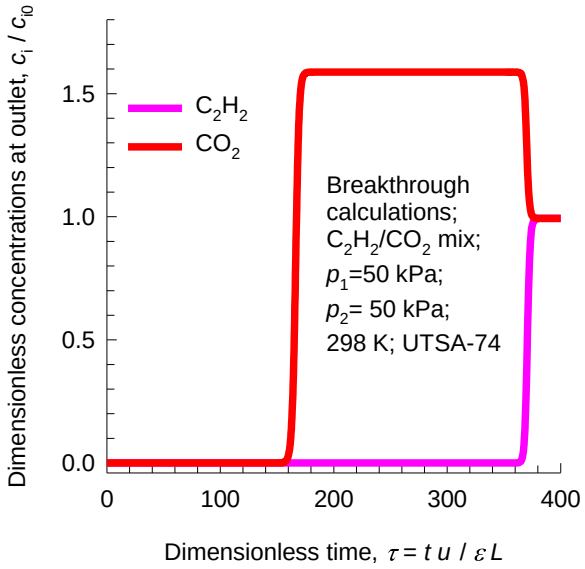


**Figure S8.** Transient breakthrough simulations for separation of equimolar $C_2H_2/CO_2$ mixture using **UTSA-74a** at 298 K, with partial pressures of 50 kPa each.

**Table S3.** Breakthrough calculations for separation of 50/50 $C_2H_2/CO_2$ mixture at 298 K.

| | Dimensionless breakthrough time $\tau_{break}$ | $C_2H_2$ adsorbed during 0-$\tau_{break}$ mol $L^{-1}$ |
|---|---|---|
| **UTSA-74a** | 362 | 4.86 |
| **UTSA-60a** | 173 | 2.33 |
| **PCP-33** | 308 | 4.16 |
| **HOF-3** | 52 | 0.7 |
| **ZnMOF-74** | 302 | 4.06 |